1

Super-Resolution Imaging

Alistair Curd[1,2], Amir Rahmani[3,4], Oliver Umney[5], Aleks Ponjavic[3,6], and Michelle Peckham[5]

[1] *Division of Pathology and Data Analytics, Faculty of Medicine and Health, University of Leeds, Leeds, UK*
[2] *School of Computing, Faculty of Engineering and Physical Sciences, University of Leeds, Leeds, UK*
[3] *School of Physics and Astronomy, Faculty of Engineering and Physical Sciences, University of Leeds, Leeds, UK*
[4] *Bragg Centre for Materials Research, University of Leeds, Leeds, UK*
[5] *School of Molecular and Cellular Biology, Faculty of Biological Sciences, University of Leeds, Leeds, UK*
[6] *School of Food Science and Nutrition, Faculty of Environment, University of Leeds, Leeds, UK*

1.1 Resolution, Widefield, and Confocal Imaging

It is widely understood that the resolution of a light microscope is limited. Any two objects that are closer together than the resolution limit cannot be discriminated as separate objects. Any point object imaged by a microscope is seen as a blurry spot (Airy disk or point spread function [PSF]). The mathematical description of resolution (x, y dimensions) of the blurry spot was first described by Abbe, in the now well-known equation: $\delta = 1/2\ (\lambda/a)$ [1], where δ is the diameter of the spot (transverse plane, full width at half maximum [FWHM]), λ is the wavelength of the excitation light, and a is the aperture. The size of the aperture depends on the numerical aperture of the objective lens, which determines the maximum angle (α) at which light can pass through the lens, and the refractive index of the immersion medium (n) as $n(\sin\alpha)$. Effectively, this means that the resolution of the microscope is approximately half the wavelength of light used to image the specimen. Typically, the highest numerical aperture of most oil-immersion lenses on fluorescence and confocal microscopes is 1.4. Thus, for an excitation wavelength of 488 nm, and a numerical aperture of 1.4, the resolution is ~180 nm. Of note, resolution is considerably worse in the axial (z) direction, where the size of the spot is equivalent to $2\lambda/n\ \sin^2\ \alpha$, or approximately 500 nm (reviewed in [2]).

Confocal fluorescence microscopy can, in principle, improve resolution slightly (about 1.4× better) compared to widefield [3, 4]. In confocal, a laser point-light source (smaller than the FWHM of the focal spot in widefield) is scanned over the field of view (FOV) and imaged via a point detector. The resolution is determined by the combination of the PSF for illumination and detection, which effectively narrows the PSF. Confocal microscopes also

Live Biological Imaging Across Scales, First Edition. Edited by Stefan Linder and Claire M. Wells.

include a pinhole between the sample and the detector to exclude out-of-focus fluorescence. Reducing the size of the pinhole improves spatial resolution in theory, but reduces light observed at the detector. The resulting image typically has a low signal-to-noise ratio (SNR), and so this approach is usually not practicable. Offsetting the point detector also improves resolution by reducing the width of the PSF, but again, the amplitude of the detected light is much smaller [5]. This idea has led to using pixel reassignment strategies to improve resolution by about twofold in confocal imaging. The displaced PSF is shifted back to its true optical axis and normalized. Using a multipoint detector, many weak signals can be reassigned and summed to generate an image with better SNR than a confocal collecting light passing through a single pinhole and with better resolution.

The idea of pixel reassignment in super-resolution imaging has led to various implementations, including the commercial instrument known as "Airyscan" confocal microscopy,[1] Re-Scan confocal microscopy [6], and home-built systems such as multifocal structured illumination microscopy [7] and instant structured illumination microscopy (iSIM) [8, 9]. These systems, combined with deconvolution of the acquired images, approximately double the resolution compared to widefield fluorescence microscopy. Axial resolution is still relatively low in these systems, but a system using two opposing lenses, and based on interference effects (4PI), has improved axial resolution to 80 nm [10] and can be used for live-cell imaging. Unfortunately, this microscope is not available commercially.

The Airyscan confocal works well for live-cell imaging. The laser power can be kept low as the Airyscan detector is highly sensitive. Multiple channels can be imaged simultaneously. It can also be used in fluorescence recovery after photobleaching (FRAP) experiments. We commonly use it for these two approaches [11, 12]. As with many live-cell imaging approaches, we would always recommend trial experiments in the first instance, to identify how fast events occur, which in turn determines the frame rates required to image your sample, and/or the size of the FOV. In the example shown here (mitochondrial dynamics; Figure 1.1), the dynamic behavior of mitochondria is relatively slow, and images taken at frame rates of 1 per second are sufficient to measure these dynamics. Many different types of labeling approaches are suitable with this approach [14] and are continuously being developed.

1.2 SR-SIM: "Super-Resolution" Structured Illumination Using Spatially Varying Illumination

One of three main approaches developed over the past 25 or so years to improve resolution is structured illumination microscopy. This approach illuminates the sample with a patterned illumination, resulting in interference effects as the pattern of light interacts with the sample. This has the overall effect of reducing spatial frequencies in the emitted signal, allowing high frequency information (which reports on smaller objects), normally excluded from the objective, to be collected. As a result, the resolution is approximately twice that of widefield [15] (~100 to 150 nm in *xy*). This approach was first commercialized by DeltaVision (OMX SR), Zeiss uses SIM in its Elyra microscopes, and Airyscan can also be considered as a form of SIM. However, the drawback of the traditional SIM approach is that the super-resolution image has to be derived computationally, and as a result, there are specific artifacts that the user needs to be aware of [16, 17].

1 See https://pages.zeiss.com/rs/896-XMS-794/images/ZEISS-Microscopy_The-Basic-Principle-of-Airyscanning.pdf

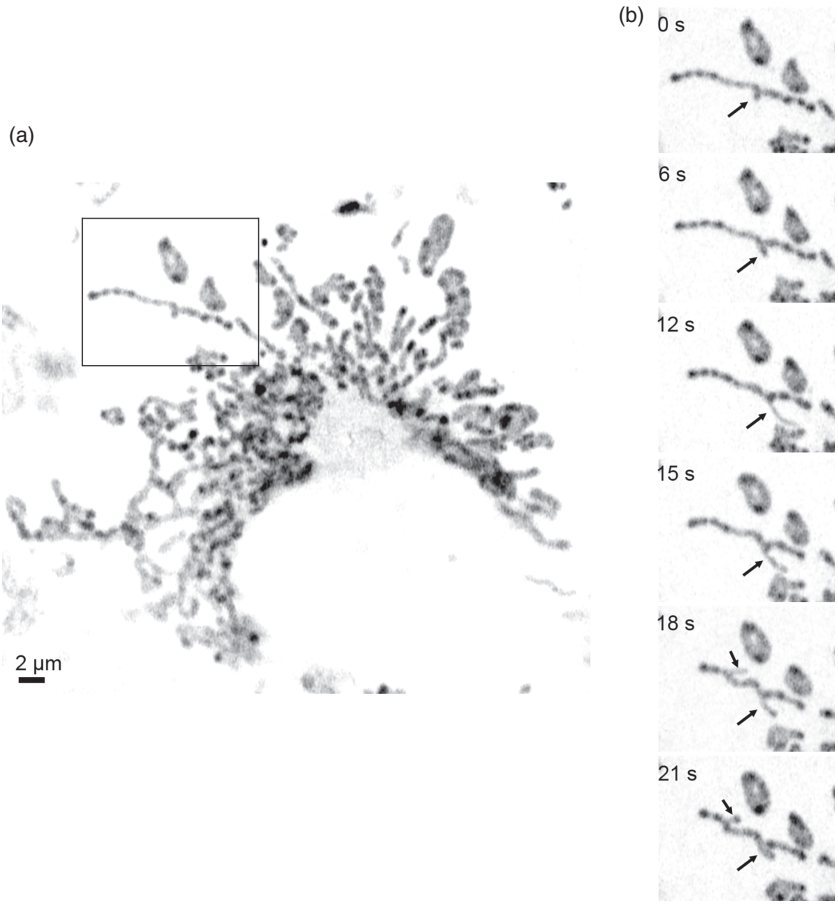

Figure 1.1 Using the Airyscan confocal for live-cell imaging. (a) Mitochondria in a living HeLa cell stained with PKmito ORANGE [13] (Abberior, Spirochrome). An inverted fluorescence image is shown. The dye is conjugated to cyclooctatetraene (COT) and labels the mitochondrial inner membrane. (b) Selected time frames from boxed area in (a), to show the dynamic behavior of a mitochondrion out toward the cell exterior. Arrows indicate changes in shape. Although this dye labels the mitochondrial cristae, these are not overly well resolved in Airyscan imaging. Scale bar is 2 µm as shown for all the images.

Multiple developments of super-resolution structured illumination microscopy (SR-SIM) have meant that this form of imaging is widely used in live-cell imaging. However, there are many different versions of this approach, many of which are "home-built" (reviewed in [18]). As the intensity of the illumination needed for imaging can be relatively low, SR-SIM allows longer-term imaging (more than 1 hour), over a wide FOV at high imaging speeds using traditional fluorophores with low bleaching rates and low cellular toxicity [18]. This approach improves imaging depth and z-resolution and has also been combined with light-sheet microscopy, which uses independent excitation and emission directions, to minimize out-of-focus excitation and improve resolution [19, 20]. Further developments of SIM have improved z-resolution to around 160 nm, with machine learning used to improve this even further for isotropic resolution of approximately 120 nm [21].

One variant of this approach, known as iSIM [9] and available commercially (Visitech) or home-built [8, 9], has also been developed. In this microscope, a lenslet array is used to generate a pattern of excitation (beamlets) that are focused on the sample. The resulting emitted light is passed back through a corresponding array of pinholes to reject out of focus light. Then the emitted light passes through a second lenslet array that scales the image of each emission spot by a factor of 0.5. A scanning mirror both scans the excitation spots across the sample, and the resulting emission spots across an sCMOS (scientific Complementary Metal-Oxide-Semiconductor) camera. This integrates and generates the final image in a single exposure. The scaling and scanning of the emitted light result in the reassignment discussed above. Like other forms of SIM, the improvement in resolution is $\sqrt{2}$, and this can be improved to twofold by image deconvolution. Here, the improvement in resolution is purely optical, the microscope is easy to use, and image capture can be very fast. However, the resultant images often have faint "scan" lines, even on the commercial system. To reduce levels of excitation even further, this approach has also been combined with machine learning, where samples are first imaged at both high and low laser powers, and machine learning is used to help reconstruct images that have only been obtained at low laser power. iSIM has also been combined with total internal reflection fluorescence microscopy (TIRFM) to improve the lateral resolution further [22] and to image at very fast frame rates (kHz).

As in other super-resolution microscopy techniques, developments of SIM have often focused on imaging the cytoskeleton and other distinctive structures such as the endoplasmic reticulum, chromosomes, and mitochondria [9, 21, 23, 24] and (see Figure 1.2). Subsequently, the dynamics of proteins and other markers important to many processes, but with less distinctive distributions, have been imaged and quantified, for instance in DNA break repair [25], endocytosis [24, 26], mitochondrial fission [27], and virus replication [28].

SIM has also benefitted from the use of machine learning to improve performance for both the more traditional versions of SIM and iSIM [29–31]. For example, residual channel attention networks (RCANs) were used in iSIM, following on from more traditional approaches such as using U-net neural networks [32], using the argument that RCANs are

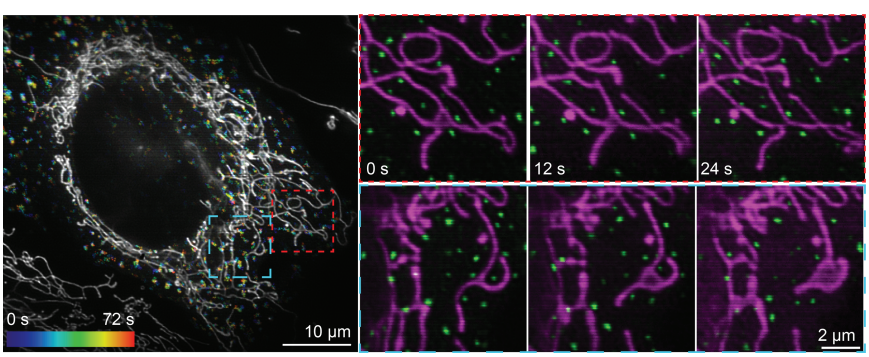

Figure 1.2 Live-cell imaging using iSIM. Cells have been transfected with Drp1 (dynamin-related protein-1)-eGFP, thought to form oligomers on mitochondria (stained using MitoTracker-red dye) to facilitate fission. Individual FOVs (red and cyan boxed regions) are shown in detail on the right-hand side.

more suited to focus on learning high-frequency information (smaller details) in images [33]. The RCAN approach was modified to use volumes of images, rather than a single image; to use a graphics processing unit (GPU) for processing and used iSIM images captured at both low and high illumination intensities for a range of cytoskeletal structures and organelles [30]. Using this approach allowed imaging of live cells for long time periods (4 hours and longer), imaging a volume approximately every 6 seconds.

1.3 STED: Stimulated Emission Depletion Microscopy

The second major approach to super-resolution imaging builds on confocal microscopy, in a technique called REversible Saturable OpticaL Fluorescent Transition (RESOLFT) microscopy [34]. When fluorophores are excited by light, the fluorophore moves from its ground (nonfluorescent) state into an excited (fluorescent) state, and the equilibrium between these two states can be modulated by light. This approach has been used to improve the resolution in other applications such as light sheet imaging [35].

In STED (stimulated emission depletion) microscopy, samples are scanned by an excitation spot to excite the fluorophores, and simultaneously by a second red-shifted laser (STED spot) with a doughnut shape. The STED spot depletes fluorescence in the region of the doughnut, only allowing fluorescence emission in the central hole of the doughnut, thus shrinking the fluorescent spot (PSF). The reduced size of the PSF thus results in higher resolution as two spots can be much closer together while still being resolvable. Of note, the STED lasers are pulsed, which helps to reduce the overall laser power. A pulsed STED laser, with a wavelength of 775 nm is typically used, and the fluorophores used emit either in the far red (excitation λ ~640 nm) or red (excitation λ ~580 nm). The resolution of a typical commercial STED microscope is ~50 nm (2–3 times better than Airyscan). A key advantage of STED is that the improvement in resolution is purely optical, although a small improvement can still be achieved by deconvolving the resulting images.

A key challenge with STED microscopy is to find suitable dyes. STED dyes need to be highly photostable, biocompatible, and able to be depleted at the appropriate wavelength. Many of the typical dyes (e.g. the Alexa dyes), or fluorescent proteins (e.g. eGFP, mCherry), used in widefield or fluorescence microscopy, do not work well in STED microscopy, although new fluorescent proteins continue to be developed to address this [36]. The two main commercial suppliers of STED microscopes (Leica and Abberior) provide a guide to suitable dyes and sample preparation.[2] Moreover, combining dyes with long and short Stokes shifts help in multicolor imaging [37]. Further probes are being developed for near-infrared STED nanoscopy [38].

Although the high intensity of the STED beam was originally thought to be incompatible with live-cell imaging, in reality, at least over a time course of about 10 minutes, it has been shown to be relatively benign [39]. In live-cell STED, proteins of interest are often tagged with self-labeling tags such as HaloTag [40] or SNAP-tags [41], which are not fluorescent until the

2 See https://www.leica-microsystems.com/science-lab/life-science/the-guide-to-sted-sample-preparation/ and https://abberior.rocks/dyes-labels/

appropriate dyes are added (see also review from [42]). Self-labeling dyes developed at Janelia[3] that are suitable for STED (e.g. for use with HaloTag or SNAP-tags), such as JF646 and JF549, are commercially available from companies such as TOCRIS, Promega, and others. Other suitable dyes are available from Abberior (https://abberior.rocks/dyes-labels/abberior-live/), including new exchangeable HaloTag ligands [43] to reduce photobleaching.

Live-cell STED has now been very successfully used by several groups [44, 45]. For example, recombinant biosensors, using self-labeling SNAP-tags have been developed to image phosphoinositides [46], and CRISPR-based knock-in has been used to endogenously label ARF GTPases using the self-labeling HaloTag [47]. This approach additionally used the ALFA tag for subsequent imaging of fixed cells using a nanobody. Moreover, combining STED with machine learning approaches has also been shown to be beneficial [30]. STED imaging is somewhat sensitive to photobleaching over extended imaging; however, reducing the intensity of the depletion laser, which in turn reduces the resolution somewhat, can help to reduce the effects of photobleaching. In addition, STED images can be further deconvolved (e.g. using Huygens [SVI] software) to slightly improve resolution and and image contrast.

In addition to self-labeling tags, cell permeant dyes have been developed for imaging a range of cytoskeletal and vesicular structures in cells, such as PKmito ORANGE to image mitochondria [13] (commercially available from Abberior: see Figure 1.3); 9-imino-10-silaxanthone (SiX) dye (with large Stokes shifts) fused to Jasplakinolide for imaging of actin; and others, such as silicon-Rhodamine (SiR) dye-labeled probes for tubulin, DNA and specific types of vesicles, including most recently, the Golgi [48]. These probes are commercially available from spirochrome.com and encompass emission wavelengths from 555 to 650 nm. The advantage of these compounds is that they can be directly added to and taken up by cells, and the targets become directly labeled within a few minutes, thus avoiding the need for transfection. However, only a small number of targets so far can be directly labelled in this way.

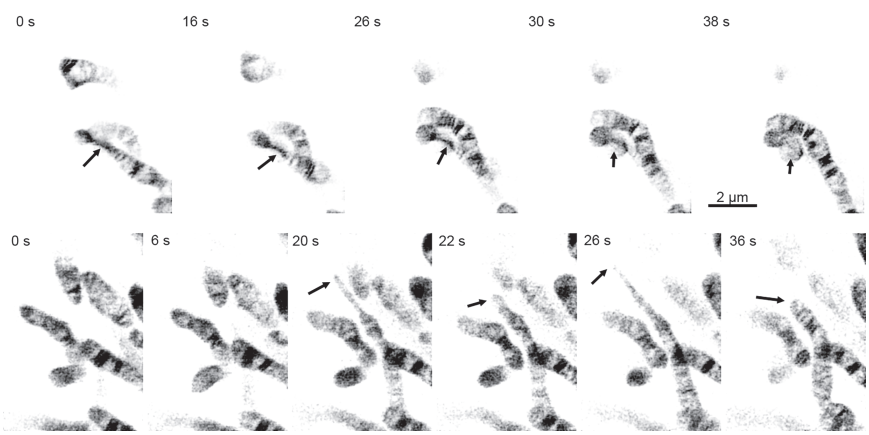

Figure 1.3 Live-cell imaging of mitochondria in HeLa Cells using STED (STEDyCon, Abberior). Frames from two sets of live-cell images are shown. Arrows show changes to mitochondrial shape. The mitochondria have been labeled with PKmito ORANGE dye (as in Figure 1.1). The resolution provided by STED (in this case ~80 nm) allows cristae within mitochondria to be resolved.

3 See https://www.janelia.org/open-science/janelia-fluor-dyes

1.4 Single Molecule Localisation Microscopies

In single-molecule imaging, the image of a single emitter formed at the detector (camera) is spread out over a number of pixels, which can be fitted using the Gaussian function to find the centroid. The precision of this fit depends on the number of detected photons and the size of the PSF. The nanoscale position of the molecule over time can be followed, as is done in single-molecule tracking (SMT). The localization precision depends on the number of photons collected, scaling as $1/\sqrt{\text{photons}}$.

The development of single-molecule tracking (SMT) in live eukaryotic cells exploited the development of total internal reflection fluorescence microscopy (TIRFM) [49]. The approach leverages the ∼200-nm evanescent wave created when a laser beam is totally reflected at a glass–water interface, such that only the cell surface is excited. It typically has a spatiotemporal resolution of 10–20 nm and 1–5 ms. By combining subsequent localizations into a track, complex dynamic information about the molecular behavior of fluorescent molecules can be extracted, such as diffusion coefficient, binding/unbinding kinetics, clustering, stoichiometry, confinement, and transitions between states [50].

We have used SMT of eGFP-tagged proteins to track the behaviour of specific proteins such as the the filopodial myosin, Myosin 10 [52, 53] (and see Figure 1.4), as well as the isolated pleckstrin homology domain from Myosin 10, which allowed us to determine binding and unbinding rates of the PH domain to the plasma membrane in cells [54]. For full-length Myosin 10, we could determine how it moves to the tip of filopodia [54]. The low abundancy of the eGFP-tagged proteins allowed us to identify single molecules and track them.

We have also applied TIRFM to demonstrate how attachment of T cells onto supposedly passivated surfaces immobilizes proteins and artificially activates the cells [55, 56]. Similar background rejection was required to image intracellular proteins, which inspired the creation of highly inclined and laminated optical sheet (HiLo) microscopy [57]. This approach uses a small (20 μm diameter) inclined laser beam to mostly restrict fluorescence excitation to the focal plane ±3 μm. To date, HiLo is the most used approach for SMT in cells and has been used in approaches focused on studying nuclear machinery due to its newfound accessibility [58–60]. Not only can mobility of molecules be extracted, but also the presence of transient structures. We have used SMT and HiLo to demonstrate the formation of individual secondary DNA structures known as G-quadruplexes in living cells (Figure 1.5a; [61]). We have also used three-dimensional SMT based on the double-helix PSF to demonstrate the varying mobility of different regions of chromatin during cell differentiation stages (Figure 1.5b); [62]).

SMT laid the foundations for the development of two further single-molecule super-resolution approaches: photoactivated localization microscopy (PALM) and stochastic optical reconstruction microscopy (STORM). In conventional fluorescence microscopy, all the fluorophores emit (ON) at the same time, and the location of individual fluorophores cannot be resolved. Single-molecule localization microscopy (SMLM) methods such as PALM and STORM overcome this limitation by only allowing a subset of the emitters to be ON in each frame, causing them to be temporally isolated and therefore minimizing the overlap between neighboring fluorophores. Both these approaches are forms of SMLM, a group of techniques that build an image of the sample over time by imaging and localizing a subset of the fluorophores in each frame [64], although these are mostly used in fixed cells.

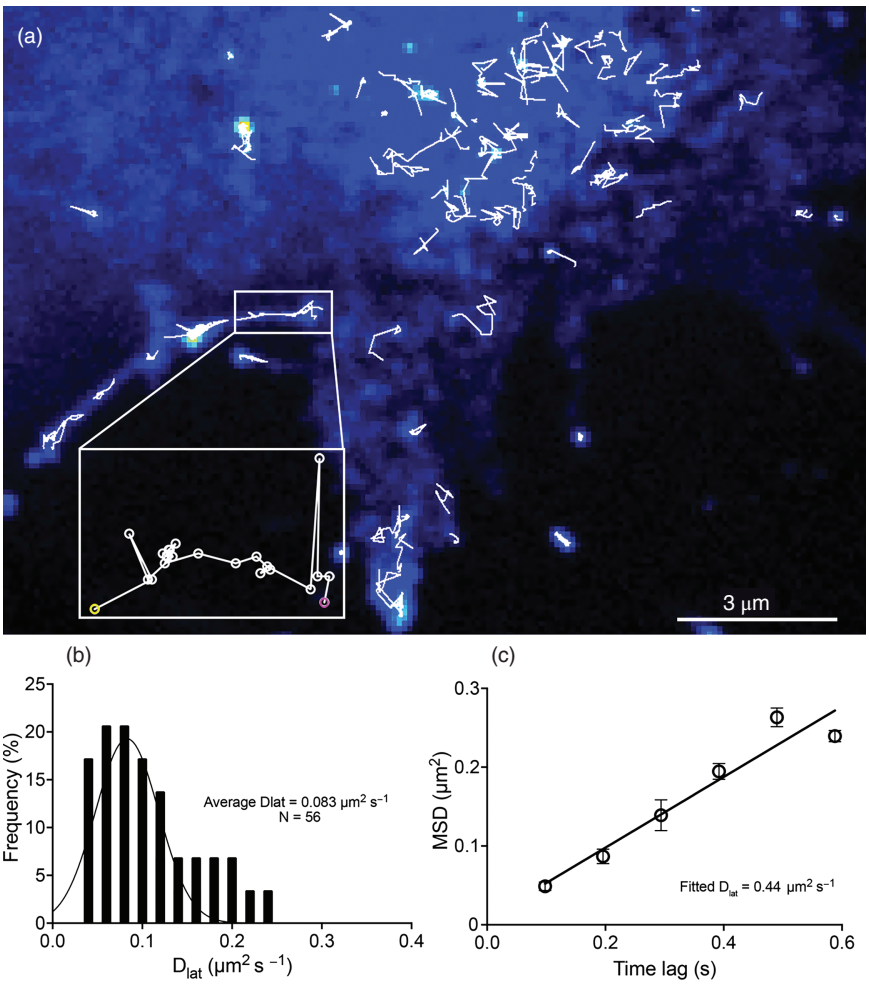

Figure 1.4 Movement of fluorescent single molecules at the plasma membrane can be tracked and analyzed. (a) Tracks for positions of individual eGFP-Myosin 10 molecules moving on the basal membrane of a cell captured using TIRFM at a frame rate of 98 frames per second. The inset shows one of these tracks in more detail for a fluorescent spot moving into a filopodium. The start position of the track is outlined in magenta and end position in yellow. (b) Data from this field of view is shown. This analysis can be performed for several experiments to estimate the distribution of the coefficients of lateral diffusion for individual eGFP-M10 molecules from many fields of view. (c) The lateral diffusion coefficient (Dlat) can be estimated from the gradient of the plot for the average mean square displacement values (MSD) versus the time lag, free from the noise affecting individual tracks (data from this experiment). For more detail, see [52–54].

PALM resulted from the development of photoactivatable GFP (PA-GFP) [65]. In this case, the sample is imaged for multiple frames and the coordinates of the ON fluorophores (PA-GFP) are determined in each, generating a super-resolution image of the cell. The level of illumination used is adjusted to only switch on a small number of GFP molecules at any one time. However, PA-GFP has a poor contrast ratio. Better fluorophores such as PAmCherry

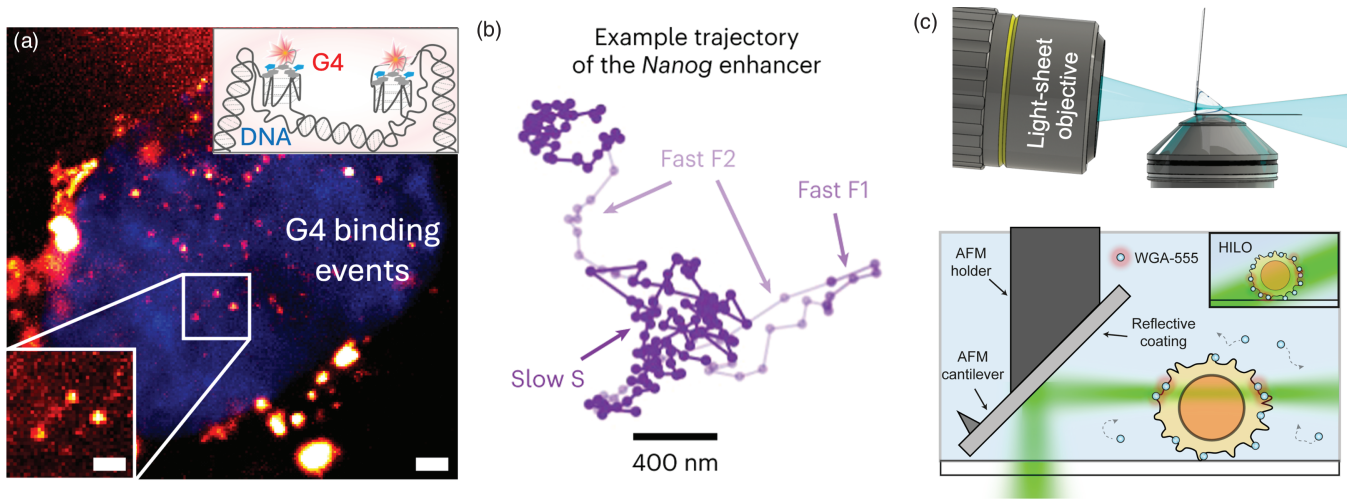

Figure 1.5 Single-molecule localization microscopy in living cells. (a) Detection of transient G-quadruplex (G4) structures using a novel dye, SiR-PyPDS, shown in red against the blue chromatin. The top inset shows a schematic of the dye binding to the G4 structures. Scale bars are 1 µm (left) and 2 µm (right). (b) Example trajectory of *Nanog* enhancer binding to chromatin undergoing multiple diffusive states, where the slow state corresponds to chromatin motion. (c) Top shows a tilted light sheet for high numerical aperture single-molecule light-sheet microscopy. Bottom shows introduction of a reflective atomic force microscopy (AFM) cantilever to achieve single-objective light-sheet microscopy for PAINT microscopy. The inset compares the excitation to HiLo excitation. *Source:* Figures adapted from PMID: [55, 61–63].

or mEos soon emerged with better contrast ratios, and consequently better performance in PALM (reviewed in [66]). Eos has the further advantage that cells expressing Eos-tagged proteins are "green" and thus expression levels can be checked, whereas cells expressing PA fluorescent proteins (PA-FPs) are not fluorescent.

STORM was developed from observations that two dyes (Cy3 and Cy5) within a very close distance exhibited blinking behavior under specific illumination conditions. Antibodies labeled with these two dyes were then used in STORM to obtain super-resolved images [67]. This was further developed into direct STORM (dSTORM) [68, 69], which showed that single organic dyes could be induced to photo-switch between OFF and ON states (blink), when irradiated in the presence of a buffer containing phosphate-buffered saline, thiols, and oxygen scavenging systems. This is a much simpler approach as it only requires a single dye (of which the "best" is still Alexa Fluor 647 [70]).

More recently, chemists realized that they could design spontaneously blinking dyes such as hydroxymethyl Si-rhodamine (HMSiR) that do not require STORM buffer to blink [71]. This has been widely adopted for live-cell imaging due to its compatibility with nontoxic buffers such as phosphate-buffered saline [72]. The slow blinking rate and limited control over on–off ratio of those dyes recently led to the development of a suite of new Janelia dyes such as JF635b with faster blinking rates and tunable on–off ratios [73], showing potential for use in a wide range of live-cell applications. A further consideration is the size of the probe used in imaging. The use of primary and secondary antibodies leads to a large linkage error [distance between the fluorophore and the object being imaged). Small probes, such as Affimers or nanobodies, are much better suited, providing a lower linkage error and better penetration into dense cytoskeletal regions [74–76].

SMLM approaches have a resolution on the order of 10–20 nm for biological structures, although for single-molecule imaging, the resolution is often more difficult to quantify. An approach used to determine resolution in electron microscopy (Fourier ring correlation) has been applied to SMLM data [77]. As noted above, localization precision depends on the number of photons collected for each localization. Most software analysis approaches enable the datasets to be filtered to exclude localizations with low precision. Finally, a further challenge is that overlapping fluorophores can also affect accurate determination of localizations. Various approaches have been developed to detect and overcome this type of behavior such as HAWK [78, 79] and more recently deep-learning (DL)-based approaches such as DEEPSTORM3D and DECODE [80, 81].

Blinking behavior can also be obtained using a single-molecule imaging technique called DNA-points accumulation for imaging in nanoscale topography (PAINT) [82]. In this case, ON/OFF switching of the fluorophores is achieved through the transient binding and unbinding of fluorophore-labeled single-stranded DNA oligonucleotides (imaging strands) that are complementary to oligonucleotides attached to the target [82, 83]. This approach has also been developed into more sophisticated approaches such as Exchange-PAINT [84)], resolution enhancement by sequential imaging (RESI) [85] and FLASH-PAINT (fluorogenic labeling in conjunction with transient adapter-mediated switching for high-throughput DNA-PAINT [86]). All of these approaches contribute to improving resolution, speed of acquisition, and multiplexing. However, they have not been widely used for live-cell imaging, due to the problem of introducing antibodies/nanobodies into cells, together

with the imaging strands [87]. However, DNA-PAINT has been adapted to perform live-cell super-resolved imaging of cellular traction forces [88].

The combination of PALM and SMT approaches provides the ability to track and image objects in live cells with high spatial and temporal resolution in an approach known as single-particle tracking (Spt) PALM. This approach still requires the fluorophores to exhibit blinking behavior, such that only a small number of objects are fluorescent at any one time and can be accurately imaged and tracked. Thus, it typically uses photoactivatable (PA) proteins such as PA-GFP or photo-switchable proteins such as mEos3 [89–91]. By activating, or switching the emission color of the FP, a subset of molecules becomes fluorescent and can then be tracked. This is an iterative process, in which molecules are activated or switched, imaged until they bleach, and then a new subset of molecules becomes activated, as in the original PALM approach. An important consideration here, as in all forms of live-cell imaging, is the frame rate. Imaging at faster frame rates increases the time resolution but reduces the number of photons per localization, and vice versa [92]. Compared to other SMLM approaches, PALM is particularly suited to live-cell imaging as the emitters are genetically encoded. However, the reactivation or switching process (illumination with 405 nm light) required for PALM imaging can be toxic to live cells. Two-color imaging is even more challenging as there are very few fluorophores that have well-separated emission spectra.

Live-cell single-molecule imaging approaches for intracellular proteins have also used a range of blinking dyes. These include trimethoprim chemical tag (TMP-tag) that is non-toxic and cell permeable coupled to a photo-switchable ATTO dye in living cells [69, 93], SNAP-tags coupled to photo-switchable dyes to image clathrin-coated pits [94], and spontaneously blinking dyes such as the fluxional dye: PFF-1, to enable live-cell imaging of organelles over periods of over 30 minutes [95] and HMSiR, to self-label SNAP-tags or HaloTags followed by imaging structures such as microtubules [71, 96]. Using dyes has the advantage that their photon output is generally much higher than fluorescent proteins, enabling more accurate fitting and tracking of single molecules. Further, it is difficult to find fluorophores that are membrane-permeable perform blinking under physiological conditions and provide the required labeling efficiencies in live cells.

1.5 Single-Molecule Light-Sheet Microscopy

While HiLo provides access into living cells, its relatively large beam thickness (6 μm), compared to the depth of field (500 nm), still produces excessive out-of-focus fluorescence that makes SMT challenging. In light-sheet microscopy, a secondary orthogonal objective lens can be used to introduce a thin (~2 μm) excitation beam, which markedly improves imaging contrast. Early work demonstrated the ability of light-sheet microscopy to greatly boost SNR in SMT, but its adoption was hampered by the need for complex custom mounting chambers [97]. This spurred on various technical developments to make light-sheet SMT more accessible, including: single-objective [98], AFM cantilever [99], and lattice light sheet [19].

We have developed two versions of single-molecule light-sheet microscopy for SMT (Figure 1.5c). To apply SMT to membrane proteins above the coverslip–cell interface, we

introduced a tilted light sheet through a low-cost chamber made from coverslips [55]. We used this to show how the behavior of T-cell membrane proteins is different in free cell membranes as compared to the coverslip–cell interface. A secondary approach was also developed to enable SMT in multiwell chambers by using a reflective AFM cantilever [63].

Note that the above light-sheet approaches rely on multiple objectives or reflective elements. More recently, remote focusing has gained popularity. This concept is used in oblique plane microscopy approaches [100–102], but challenges remain in terms of maximizing the optical transfer efficiency of the systems as the large number of elements within the system reduces photon collection that is crucial for SMT.

1.6 Computation for Live-Cell Super Resolution

Images are data, and a wide range of computational approaches is used to help generate images and analyze them. Computational methods in super-resolution microscopy are used in many ways to improve spatial and temporal resolutions beyond that of the raw acquired data. They are intrinsic to reconstructing an image from SIM, as discussed above [16, 17], and are essential for acquiring particle localizations from fluorescent emitters in SMLM and tracking applications [103]. In live-cell SMLM imaging, acquiring as many localizations as possible per frame becomes particularly important, and algorithms have been developed to improve the trade-off between localization accuracy and precision and the density of emitters [80, 81]. Since nearby bright emitters can easily result in incorrect localizations (e.g. one localization resulting from two bright molecules at their mean position), research software also exists to check for and mitigate these errors [78, 79].

Super-resolution optical fluctuation imaging (SOFI) [104] and super-resolution radial fluctuations (SRRFs) [105, 106] are two computational methods which take widefield image sequences (several frames per time point) and analyze their intensity variations over time. SOFI uses correlations between images over time to enhance fluorescence intensity peaks and makes use of the fact that intensity fluctuations arising from different emitting molecules are uncorrelated. SRRF enhances intensity peaks by finding the degree of convergence of intensity gradients across an FOV and uses temporal correlations to reduce noise in the result. Both SOFI and SRRF can result in image resolutions under 100 nm, but performance may depend on the spatial distribution of the fluorescence signal and the computational techniques can result in nonlinear accentuation of bright features. They can also be used in conjunction with super-resolution (e.g. SIM) or volumetric data acquisition methods (e.g. multifocal microscopy) to result in further increases in resolution in 2D or 3D [105, 107].

Even with techniques where a super-resolution image is obtained before any computation (e.g. STED, iSIM) single-image deconvolution, denoising and other algorithms can further enhance spatial and temporal resolutions, as reviewed in ([108]. Deconvolution enhances the SNR at higher spatial frequencies in an image, allowing more detail to be discerned, although it can over-sharpen an image and cause some ringing artifacts if applied incorrectly [109]. Some commercial instruments are supplied with image deconvolution software, and commercial deconvolution software is available, as free, open source software [110]. Often, the user provides information about the shape of the native PSF of the system as input, and the output is a deconvolved image.

More recently, many methods have used supervised DL to reconstruct high-quality data from low-quality data without an explicit model, instead learning directly from the data, as reviewed in [108, 111]. As mentioned above for iSIM, this approach typically uses pairs of low-resolution and super-resolution data. For denoising, these image pairs are often high-SNR and low-SNR images, although pairs of images under identical conditions and even single images can be used for some improvement [112]. After training, a DL algorithm converts other low-SNR images to high-SNR equivalents. This allows imaging at lower laser powers, which enables gentle imaging for longer periods of time in live samples, and is followed by image reconstruction approaches [113–115]. When representative image pairs can be captured, it is even possible to convert images from a lower-resolution technique (e.g. widefield, confocal, SIM) to their predicted equivalents if a higher-resolution technique had been used (e.g. STED) [116].

The benefits of image enhancement with DL are very attractive, but great care must be taken when training an algorithm and interpreting the output. When training data have included enough sufficiently similar features to the input images in a real live-cell experiment, the expected output is faithful images of the underlying fluorescence distribution with enhanced resolution. However, when the input images contain features that are not within the domain of the training dataset, the DL algorithm may often "hallucinate" an incorrect resolution-enhanced region, adding or removing intensity in a certain pattern. We may expect this to be the case to some extent in live-cell fluorescence imaging, when protein distributions are irregular to some extent and different in detail from sample to sample and from time point to time point. The larger the training dataset, the fewer hallucination errors there should be. All of the DL references in this section contain examples of such errors, and thorough training and testing of algorithms is advised, as well as rigor in drawing conclusions from the output in experiments.

1.7 Advanced Applications in Cells

Finally, the field of high-resolution imaging is a rapidly developing field. A key example of this is the recent development of the localization-based super-resolution technique known as MINFLUX [117–120], which has been used in vitro and in cells. The resolution of this approach, in tracking, is close to 1 nm, which has allowed a detailed analysis of how kinesin (and other motors) step along microtubule tracks (8-nm-sized steps). Its reduced photon requirement compared to conventional SMLM techniques is particularly advantageous for imaging. It uses a point-scanning excitation approach using a doughnut-shaped beam to probe the position of the fluorescent emitter. Notably, localization in MINFLUX is not based on the fitting of a model function to PSF, but rather on the fluorescence emission signal from the emitter captured during the scanning cycle. The position of the fluorophore single emitter can be identified using a triangulation scanning approach to identify a fluorescence intensity signal that has a local minimum where the target is located. During the scanning cycle with a patterned excitation beam (doughnut-shaped beam), the fluorescence emission from the emitter would vary as a response to the variation of the excitation beam intensity. Applying MINFLUX for live-cell imaging requires photostable fluorophores over the range of milliseconds to ensure the changes in the fluorescence intensity

estimate the position correctly and consequently result in precise MINFLUX imaging. In addition to needing a photostable fluorophore, it is essential to use effective drift correction and focus stabilization techniques [121, 122]. Any instability in the system would impact the localization precision and ultimately the resolution that MINFLUX designed to achieve.

1.8 Concluding Remarks

The choice of live-cell super-resolution microscopy technique depends critically on the specific biological question being addressed. This chapter has highlighted the unique capabilities and limitations of several approaches that have been developed over the past few years. We hope this will provide some guidance alongside the many reviews on super-resolution imaging [111, 123–125]. While each technique offers advantages and limitations, the convergence of advanced optical designs, machine-learning-assisted approaches, and ever-improving fluorescent probes promises further advancements in these areas that will lead to greater spatiotemporal resolution, enabling the detailed study of dynamic cellular processes with unprecedented information.

Acknowledgments

We would like to acknowledge the funding from BBSRC Alert (for the STED and single-molecule microscope) and the Wellcome Trust for the inverted Airyscan confocal microscope, as well as the highly supportive staff in the BioImaging Facility (Ruth Hughes and Sally Boxall) in maintaining, training, and supporting the microscopes.

References

1 Abbe, E. (1881). On the estimation of aperture in the microscope. *J. R. Microsc. Soc.* 1: 388–423.
2 Hell, S.W., Dyba, M., and Jakobs, S. (2004). Concepts for nanoscale resolution in fluorescence microscopy. *Curr. Opin. Neurobiol.* 14 (5): 599–609.
3 Brakenhoff, G.J., Blom, P., and Barends, P. (1979). Confocal scanning light microscopy with high aperture immersion lenses. *J. Microsc.* 117: 219–232.
4 Wilson, T. and Sheppard, C.J.R. (1984). *Theory and Practice of Scanning Optical Microscopy*. New York: Academic.
5 Sheppard, C.J.R. (1988). Super-resolution in confocal imaging. *Optik* 80: 53–54.
6 De Luca, G.M., Breedijk, R.M., Brandt, R.A. et al. (2013). Re-scan confocal microscopy: scanning twice for better resolution. *Biomed. Opt. Express* 4 (11): 2644–2656.
7 York, A.G., Parekh, S.H., Dalle Nogare, D. et al. (2012). Resolution doubling in live, multicellular organisms via multifocal structured illumination microscopy. *Nat. Methods* 9 (7): 749–754.

8 Curd, A., Cleasby, A., Makowska, K. et al. (2015). Construction of an instant structured illumination microscope. *Methods* 88: 37–47.
9 York, A.G., Chandris, P., Nogare, D.D. et al. (2013). Instant super-resolution imaging in live cells and embryos via analog image processing. *Nat. Methods* 10 (11): 1122–1126.
10 Hell, S.W. (2003). Toward fluorescence nanoscopy. *Nat. Biotechnol.* 21 (11): 1347–1355.
11 Casas-Mao, D., Carrington, G., Pujol, M.G., and Peckham, M. (2024). Effects of specific disease mutations in non-muscle myosin 2A on its structure and function. *J. Biol. Chem.* 300 (1): 105514.
12 Lopata, A., Hughes, R., Tiede, C. et al. (2018). Affimer proteins for F-actin: novel affinity reagents that label F-actin in live and fixed cells. *Sci. Rep.* 8 (1): 6572.
13 Liu, T., Stephan, T., Chen, P. et al. (2022). Multi-color live-cell STED nanoscopy of mitochondria with a gentle inner membrane stain. *Proc. Natl. Acad. Sci. USA* 119 (52): e2215799119.
14 Specht, E.A., Braselmann, E., and Palmer, A.E. (2017). A critical and comparative review of fluorescent tools for live-cell imaging. *Annu. Rev. Physiol.* 79: 93–117.
15 Gustafsson, M.G. (2000). Surpassing the lateral resolution limit by a factor of two using structured illumination microscopy. *J. Microsc.* 198 (Pt 2): 82–87.
16 Ball, G., Demmerle, J., Kaufmann, R. et al. (2015). SIMcheck: a toolbox for successful super-resolution structured illumination microscopy. *Sci. Rep.* 5: 15915.
17 Demmerle, J., Innocent, C., North, A.J. et al. (2017). Strategic and practical guidelines for successful structured illumination microscopy. *Nat. Protoc.* 12 (5): 988–1010.
18 Wu, Y. and Shroff, H. (2018). Faster, sharper, and deeper: structured illumination microscopy for biological imaging. *Nat. Methods* 15 (12): 1011–1019.
19 Chen, B.C., Legant, W.R., Wang, K. et al. (2014). Lattice light-sheet microscopy: imaging molecules to embryos at high spatiotemporal resolution. *Science* 346 (6208): 1257998.
20 Chen, B., Chang, B.J., Roudot, P. et al. (2022). Resolution doubling in light-sheet microscopy via oblique plane structured illumination. *Nat. Methods* 19 (11): 1419–1426.
21 Li, X., Wu, Y., Su, Y. et al. (2023). Three-dimensional structured illumination microscopy with enhanced axial resolution. *Nat. Biotechnol.* 41 (9): 1307–1319.
22 Guo, M., Chandris, P., Giannini, J.P. et al. (2018). Single-shot super-resolution total internal reflection fluorescence microscopy. *Nat. Methods* 15 (6): 425–428.
23 Kner, P., Chhun, B.B., Griffis, E.R. et al. (2009). Super-resolution video microscopy of live cells by structured illumination. *Nat. Methods* 6 (5): 339–342.
24 Gao, L., Shao, L., Higgins Christopher, D. et al. (2012). Noninvasive imaging beyond the diffraction limit of 3D dynamics in thickly fluorescent specimens. *Cell* 151 (6): 1370–1385.
25 Lesterlin, C., Ball, G., Schermelleh, L., and Sherratt, D.J. (2014). RecA bundles mediate homology pairing between distant sisters during DNA break repair. *Nature* 506 (7487): 249–253.
26 Li, D., Shao, L., Chen, B.-C. et al. (2015). Extended-resolution structured illumination imaging of endocytic and cytoskeletal dynamics. *Science* 349 (6251): aab3500.
27 Kleele, T., Rey, T., Winter, J. et al. (2021). Distinct fission signatures predict mitochondrial degradation or biogenesis. *Nature* 593 (7859): 435–439.

28 Remenyi, R., Gao, Y., Hughes, R.E. et al. (2018). Persistent replication of a Chikungunya virus replicon in human cells is associated with presence of stable cytoplasmic granules containing nonstructural protein 3. *J. Virol.* 92 (16).

29 Ward, E.N., Hecker, L., Christensen, C.N. et al. (2022). Machine learning assisted interferometric structured illumination microscopy for dynamic biological imaging. *Nat. Commun.* 13 (1): 7836.

30 Chen, J., Sasaki, H., Lai, H. et al. (2021). Three-dimensional residual channel attention networks denoise and sharpen fluorescence microscopy image volumes. *Nat. Methods* 18 (6): 678–687.

31 Jin, L., Liu, B., Zhao, F. et al. (2020). Deep learning enables structured illumination microscopy with low light levels and enhanced speed. *Nat. Commun.* 11 (1): 1934.

32 Ronneberger, O., Fischer, P., and Brox, T. (2015). U-Net: convolutional networks for biomedical image segmentation. In: *Medical Image Computing and Computer-Assisted Intervention—MICCAI 2015* (ed. N. Navab, H. Hornegger, W.M. Wells, and A. Frangi). Springer.

33 Zhang Y, Li K, Li K, Wang L, Zhong B, Fu Y. Image super-resolution using very deep residual channel attention networks. *arXiv:180702758v2*. 2018.

34 Hell, S.W., Jakobs, S., and Kastrup, L. (2003). Imaging and writing at the nanoscale with focused visible light through saturable optical transitions. *Appl. Phys. A* 77: 859–860.

35 Hoyer, P., de Medeiros, G., Balazs, B. et al. (2016). Breaking the diffraction limit of light-sheet fluorescence microscopy by RESOLFT. *Proc. Natl. Acad. Sci. USA* 113 (13): 3442–3446.

36 Jeong, S., Widengren, J., and Lee, J.C. (2021). Fluorescent probes for STED optical nanoscopy. *Nanomaterials (Basel).* 12 (1): 21.

37 Sednev, M.V., Belov, V.N., and Hell, S.W. (2015). Fluorescent dyes with large stokes shifts for super-resolution optical microscopy of biological objects: a review. *Methods Appl Fluoresc.* 3 (4): 042004.

38 Kamper, M., Ta, H., Jensen, N.A. et al. (2018). Near-infrared STED nanoscopy with an engineered bacterial phytochrome. *Nat. Commun.* 9 (1): 4762.

39 Kilian, N., Goryaynov, A., Lessard, M.D. et al. (2018). Assessing photodamage in live-cell STED microscopy. *Nat. Methods* 15 (10): 755–756.

40 Los, G.V., Encell, L.P., McDougall, M.G. et al. (2008). HaloTag: a novel protein labeling technology for cell imaging and protein analysis. *ACS Chem. Biol.* 3 (6): 373–382.

41 Juillerat, A., Gronemeyer, T., Keppler, A. et al. (2003). Directed evolution of O6-alkylguanine-DNA alkyltransferase for efficient labeling of fusion proteins with small molecules in vivo. *Chem. Biol.* 10 (4): 313–317.

42 Crivat, G. and Taraska, J.W. (2012). Imaging proteins inside cells with fluorescent tags. *Trends Biotechnol.* 30 (1): 8–16.

43 Kompa, J., Bruins, J., Glogger, M. et al. (2023). Exchangeable HaloTag ligands for super-resolution fluorescence microscopy. *J. Am. Chem. Soc.* 145 (5): 3075–3083.

44 Stockhammer, A. and Bottanelli, F. (2021). Appreciating the small things in life: STED microscopy in living cells. *J. Phys. D. Appl. Phys.* 54: 033001.

45 Carsten, A., Failla, A.V., and Aepfelbacher, M. (2024). MINFLUX nanoscopy: Visualising biological matter at the nanoscale level. *J. Microsc.* 298 (2): 219–231.

46 Maib, H., Adarska, P., Hunton, R. et al. (2024). Recombinant biosensors for multiplex and super-resolution imaging of phosphoinositides. *J. Cell Biol.* 223 (6): e202310095.

47 Gotzke, H., Kilisch, M., Martinez-Carranza, M. et al. (2019). The ALFA-tag is a highly versatile tool for nanobody-based bioscience applications. *Nat. Commun.* 10 (1): 4403.

48 Saidjalolov, S., Chen, X.-X., Moreno, J. et al. (2024). Asparagusic Golgi Trackers. *J. Am. Chem. Soc.* 4 (10): 3759–3765.

49 Axelrod, D. (2001). Total internal reflection fluorescence microscopy in cell biology. *Traffic* 2 (11): 764–774.

50 Elf, J. and Barkefors, I. (2019). Single-molecule kinetics in living cells. *Annu. Rev. Biochem.* 88: 635–659.

51 Zhang, Y., Ling, J., Liu, T., and Chen, Z. (2024). Lumos maxima - How robust fluorophores resist photobleaching? *Curr. Opin. Chem. Biol.* 79: 102439.

52 Mashanov, G.I., Tacon, D., Knight, A.E. et al. (2003). Visualizing single molecules inside living cells using total internal reflection fluorescence microscopy. *Methods* 29 (2): 142–152.

53 Baboolal, T.G., Mashanov, G.I., Nenasheva, T.A. et al. (2016). A combination of diffusion and active translocation localizes myosin 10 to the filopodial tip. *J. Biol. Chem.* 291 (43): 22373–22385.

54 Mashanov, G.I., Tacon, D., Peckham, M., and Molloy, J.E. (2004). The spatial and temporal dynamics of pleckstrin homology domain binding at the plasma membrane measured by imaging single molecules in live mouse myoblasts. *J. Biol. Chem.* 279 (15): 15274–15280.

55 Ponjavic, A., McColl, J., Carr, A.R. et al. (2018). Single-molecule light-sheet imaging of suspended T cells. *Biophys. J.* 114 (9): 2200–2211.

56 Santos, A.M., Ponjavic, A., Fritzsche, M. et al. (2018). Capturing resting T cells: the perils of PLL. *Nat. Immunol.* 19 (3): 203–205.

57 Tokunaga, M., Imamoto, N., and Sakata-Sogawa, K. (2008). Highly inclined thin illumination enables clear single-molecule imaging in cells. *Nat. Methods* 5 (2): 159–161.

58 Chong, S., Dugast-Darzacq, C., Liu, Z. et al. (2018). Imaging dynamic and selective low-complexity domain interactions that control gene transcription. *Science* 361 (6400): eaar2555.

59 Nozaki, T., Imai, R., Tanbo, M. et al. (2017). Dynamic Organization of Chromatin Domains Revealed by Super-Resolution Live-Cell Imaging. *Mol. Cell* 67 (2): 282–293.

60 Hansen, A.S., Pustova, I., Cattoglio, C. et al. (2017). CTCF and cohesin regulate chromatin loop stability with distinct dynamics. *elife* 6: e25776.

61 Di Antonio, M., Ponjavic, A., Radzevicius, A. et al. (2020). Single-molecule visualization of DNA G-quadruplex formation in live cells. *Nat. Chem.* 12 (9): 832–837.

62 Basu, S., Shukron, O., Hall, D. et al. (2023). Live-cell three-dimensional single-molecule tracking reveals modulation of enhancer dynamics by NuRD. *Nat. Struct. Mol. Biol.* 30 (11): 1628–1639.

63 Ponjavic, A., Ye, Y., Laue, E. et al. (2018). Sensitive light-sheet microscopy in multiwell plates using an AFM cantilever. *Biomed. Opt. Express* 9 (12): 5863–5880.

64 Lelek, M., Gyparaki, M.T., Beliu, G. et al. (2021). Single-molecule localization microscopy. *Nat Rev Methods Primers.* 1: 39.

65 Betzig, E., Patterson, G.H., Sougrat, R. et al. (2006). Imaging intracellular fluorescent proteins at nanometer resolution. *Science* 313 (5793): 1642–1645.

66 Shcherbakova, D.M., Sengupta, P., Lippincott-Schwartz, J., and Verkhusha, V.V. (2014). Photocontrollable fluorescent proteins for superresolution imaging. *Annu. Rev. Biophys.* 43: 303–329.

67 Rust, M.J., Bates, M., and Zhuang, X. (2006). Sub-diffraction-limit imaging by stochastic optical reconstruction microscopy (STORM). *Nat. Methods* 3 (10): 793–795.

68 Heilemann, M., van de Linde, S., Schuttpelz, M. et al. (2008). Subdiffraction-resolution fluorescence imaging with conventional fluorescent probes. *Angew. Chem. Int. Ed. Engl.* 47 (33): 6172–6176.

69 Heilemann, M., van de Linde, S., Mukherjee, A., and Sauer, M. (2009). Super-resolution imaging with small organic fluorophores. *Angew. Chem. Int. Ed. Engl.* 48 (37): 6903–6908.

70 Bates, M., Huang, B., Dempsey, G.T., and Zhuang, X. (2007). Multicolor super-resolution imaging with photo-switchable fluorescent probes. *Science* 317 (5845): 1749–1753.

71 Uno, S.N., Kamiya, M., Yoshihara, T. et al. (2014). A spontaneously blinking fluorophore based on intramolecular spirocyclization for live-cell super-resolution imaging. *Nat. Chem.* 6 (8): 681–689.

72 Werther, P., Yserentant, K., Braun, F. et al. (2020). Live-cell localization microscopy with a fluorogenic and self-blinking tetrazine probe. *Angew. Chem. Int. Ed. Engl.* 59 (2): 804–810.

73 Holland KL, Plutkis SE, Daugird TA, Sau A, Grimm JB, English BP, et al. A series of spontaneously blinking dyes for super-resolution microscopy. *bioRxiv*. 2024.

74 Carrington, G., Tomlinson, D., and Peckham, M. (2019). Exploiting nanobodies and Affimers for superresolution imaging in light microscopy. *Mol. Biol. Cell* 30 (22): 2737–2740.

75 Cordell, P., Carrington, G., Curd, A. et al. (2022). Affimers and nanobodies as molecular probes and their applications in imaging. *J. Cell Sci.* 135 (14).

76 Liu, S., Hoess, P., and Ries, J. (2022). Super-resolution microscopy for structural cell biology. *Annu. Rev. Biophys.* 51: 301–326.

77 Nieuwenhuizen, R.P., Lidke, K.A., Bates, M. et al. (2013). Measuring image resolution in optical nanoscopy. *Nat. Methods* 10 (6): 557–562.

78 Marsh, R.J., Costello, I., Gorey, M.A. et al. (2021). Sub-diffraction error mapping for localisation microscopy images. *Nat. Commun.* 12 (1): 5611.

79 Marsh, R.J., Pfisterer, K., Bennett, P. et al. (2018). Artifact-free high-density localization microscopy analysis. *Nat. Methods* 15 (9): 689–692.

80 Nehme, E., Freedman, D., Gordon, R. et al. (2020). DeepSTORM3D: dense 3D localization microscopy and PSF design by deep learning. *Nat. Methods* 17 (7): 734–740.

81 Speiser, A., Muller, L.R., Hoess, P. et al. (2021). Deep learning enables fast and dense single-molecule localization with high accuracy. *Nat. Methods* 18 (9): 1082–1090.

82 Jungmann, R., Steinhauer, C., Scheible, M. et al. (2010). Single-molecule kinetics and super-resolution microscopy by fluorescence imaging of transient binding on DNA origami. *Nano Lett.* 10 (11): 4756–4761.

83 Sharonov, A. and Hochstrasser, R.M. (2006). Wide-field subdiffraction imaging by accumulated binding of diffusing probes. *Proc. Natl. Acad. Sci. USA* 103 (50): 18911–18916.

84 Jungmann, R., Avendano, M.S., Woehrstein, J.B. et al. (2014). Multiplexed 3D cellular super-resolution imaging with DNA-PAINT and Exchange-PAINT. *Nat. Methods* 11 (3): 313–318.

85 Reinhardt, S.C.M., Masullo, L.A., Baudrexel, I. et al. (2023). Angstrom-resolution fluorescence microscopy. *Nature* 617 (7962): 711–716.

86 Schueder, F., Rivera-Molina, F., Su, M. et al. (2024). Unraveling cellular complexity with transient adapters in highly multiplexed super-resolution imaging. *Cell* 187 (7): 1769–84 e18.

87 Strauss, S., Nickels, P.C., Strauss, M.T. et al. (2018). Modified aptamers enable quantitative sub-10-nm cellular DNA-PAINT imaging. *Nat. Methods* 15 (9): 685–688.

88 Brockman, J.M., Su, H., Blanchard, A.T. et al. (2020). Live-cell super-resolved PAINT imaging of piconewton cellular traction forces. *Nat. Methods* 17 (10): 1018–1024.

89 Pandzic, E., Rossy, J., and Gaus, K. (2015). Tracking molecular dynamics without tracking: image correlation of photo-activation microscopy. *Methods Appl Fluoresc.* 3 (1): 014006.

90 Manley, S., Gillette, J.M., and Lippincott-Schwartz, J. (2010). Single-particle tracking photoactivated localization microscopy for mapping single-molecule dynamics. *Methods Enzymol.* 475: 109–120.

91 Manley, S., Gillette, J.M., Patterson, G.H. et al. (2008). High-density mapping of single-molecule trajectories with photoactivated localization microscopy. *Nat. Methods* 5 (2): 155–157.

92 Henriques, R., Griffiths, C., Hesper Rego, E., and Mhlanga, M.M. (2011). PALM and STORM: unlocking live-cell super-resolution. *Biopolymers* 95 (5): 322–331.

93 Wombacher, R., Heidbreder, M., van de Linde, S. et al. (2010). Live-cell super-resolution imaging with trimethoprim conjugates. *Nat. Methods* 7 (9): 717–719.

94 Jones, S.A., Shim, S.H., He, J., and Zhuang, X. (2011). Fast, three-dimensional super-resolution imaging of live cells. *Nat. Methods* 8 (6): 499–508.

95 Halabi, E.A., Pinotsi, D., and Rivera-Fuentes, P. (2019). Photoregulated fluxional fluorophores for live-cell super-resolution microscopy with no apparent photobleaching. *Nat. Commun.* 10 (1): 1232.

96 Tang, Q., Sensale, S., Bond, C. et al. (2023). Interplay between stochastic enzyme activity and microtubule stability drives detyrosination enrichment on microtubule subsets. *Curr. Biol.* 33: 5169–84.e8.

97 Ritter, J.G., Veith, R., Veenendaal, A. et al. (2010). Light sheet microscopy for single molecule tracking in living tissue. *PLoS One* 5 (7): e11639.

98 Galland, R., Grenci, G., Aravind, A. et al. (2015). 3D high- and super-resolution imaging using single-objective SPIM. *Nat. Methods* 12 (7): 641–644.

99 Gebhardt, J.C., Suter, D.M., Roy, R. et al. (2013). Single-molecule imaging of transcription factor binding to DNA in live mammalian cells. *Nat. Methods* 10 (5): 421–426.

100 Yang, B., Chen, X., Wang, Y. et al. (2019). Epi-illumination SPIM for volumetric imaging with high spatial-temporal resolution. *Nat. Methods* 16 (6): 501–504.

101 Sapoznik, E., Chang, B.J., Huh, J. et al. (2020). A versatile oblique plane microscope for large-scale and high-resolution imaging of subcellular dynamics. *elife* 9.

102 Kim, J., Wojcik, M., Wang, Y. et al. (2019). Oblique-plane single-molecule localization microscopy for tissues and small intact animals. *Nat. Methods* 16 (9): 853–857.

103 Sage, D., Pham, T.-A., Babcock, H. et al. (2019). Super-resolution fight club: assessment of 2D and 3D single-molecule localization microscopy software. *Nat. Methods* 16 (5): 387–395.

104 Dertinger, T., Colyer, R., Iyer, G. et al. (2009). Fast, background-free, 3D super-resolution optical fluctuation imaging (SOFI). *Proc. Natl. Acad. Sci.* 106 (52): 22287–22292.

105 Laine, R.F., Heil, H.S., Coelho, S. et al. (2023). High-fidelity 3D live-cell nanoscopy through data-driven enhanced super-resolution radial fluctuation. *Nat. Methods* 20 (12): 1949–1956.

106 Gustafsson, N., Culley, S., Ashdown, G. et al. (2016). Fast live-cell conventional fluorophore nanoscopy with ImageJ through super-resolution radial fluctuations. *Nat. Commun.* 7 (1): 12471.

107 Descloux, A.C., Grußmayer, K.S., Navikas, V. et al. (2021). Experimental combination of super-resolution optical fluctuation imaging with structured illumination microscopy for large fields-of-view. *ACS Photonics.* 8 (8): 2440–2449.

108 Shroff, H., Testa, I., Jug, F., and Manley, S. (2024). Live-cell imaging powered by computation. *Nat. Rev. Mol. Cell Biol.* 25 (6): 443–463.

109 Sarder, P. and Nehorai, A. (2006). Deconvolution methods for 3-D fluorescence microscopy images. *IEEE Signal Process. Mag.* 23 (3): 32–45.

110 Sage, D., Donati, L., Soulez, F. et al. (2017). DeconvolutionLab2: an open-source software for deconvolution microscopy. *Methods* 115: 28–41.

111 Pylvanainen, J.W., Gomez-de-Mariscal, E., Henriques, R., and Jacquemet, G. (2023). Live-cell imaging in the deep learning era. *Curr. Opin. Cell Biol.* 85: 102271.

112 Alexander Krull, Tim-Oliver Buchholz, Florian Jug. (2019) Noise2Void - Learning denoising from single noisy Images. *Proceedings of the IEEE Conference on Computer Vision and Pattern Recognition* (2129–137).

113 Qiao, C., Li, D., Guo, Y. et al. (2021). Evaluation and development of deep neural networks for image super-resolution in optical microscopy. *Nat. Methods* 18 (2): 194–202.

114 Chen, R., Tang, X., Zhao, Y. et al. (2023). Single-frame deep-learning super-resolution microscopy for intracellular dynamics imaging. *Nat. Commun.* 14 (1): 2854.

115 Weigert M, Schmidt U, Boothe T, Müller A, Dibrov A, et al. Content-aware image restoration: pushing the limits of fluorescence microscopy. *bioRxiv*. 2017.

116 Wang, H., Rivenson, Y., Jin, Y. et al. (2019). Deep learning enables cross-modality super-resolution in fluorescence microscopy. *Nat. Methods* 16 (1): 103–110.

117 Balzarotti, F., Eilers, Y., Gwosch, K.C. et al. (2017). Nanometer resolution imaging and tracking of fluorescent molecules with minimal photon fluxes. *Science* 355 (6325): 606–612.

118 Deguchi, T., Iwanski, M.K., Schentarra, E.M. et al. (2023). Direct observation of motor protein stepping in living cells using MINFLUX. *Science* 379 (6636): 1010–1015.

119 Wirth, J.O., Schentarra, E.M., Scheiderer, L. et al. (2024). Uncovering kinesin dynamics in neurites with MINFLUX. *Commun Biol.* 7 (1): 661.

120 Wirth, J.O., Scheiderer, L., Engelhardt, T. et al. (2023). MINFLUX dissects the unimpeded walking of kinesin-1. *Science* 379 (6636): 1004–1010.

121 Coelho, S., Baek, J., Walsh, J. et al. (2021). 3D active stabilization for single-molecule imaging. *Nat. Protoc.* 16 (1): 497–515.

122 Rahmani, A., Cox, T., Achary, A.T.A., and Ponjavic, A. (2024). Astigmatism-based active focus stabilisation with universal objective lens compatibility, extended operating range and nanometer precision. *Opt. Express* 32 (8): 13331–13341.

123 D'Este, E., Lukinavicius, G., Lincoln, R. et al. (2024). Advancing cell biology with nanoscale fluorescence imaging: essential practical considerations. *Trends Cell Biol.* 34 (8): 671–684.

124 Hugelier, S., Colosi, P.L., and Lakadamyali, M. (2023). Quantitative single-molecule localization microscopy. *Annu. Rev. Biophys.* 52: 139–160.

125 Jacquemet, G., Carisey, A.F., Hamidi, H. et al. (2020). The cell biologist's guide to super-resolution microscopy. *J. Cell Sci.* 133 (11): jcs240713.